The LysM Receptor-Like Kinase SlLYK10 Controls Lipochitooligosaccharide Signaling in Inner Cell Layers of Tomato Roots

Yi Ding, Tongming Wang, Virginie Gasciolli, Guilhem Reyt, Céline Remblière, Fabien Marcel, Tracy François, Abdelhafid Bendahmane, Guanghua He, Jean Jacques Bono, et al.

The LysM receptor-like kinase SlLYK10 controls lipochitooligosaccharide responses in inner cell layers of tomato roots

Running Title : **SlLYK10 controls Ca spiking in inner root cells**

Authors:

Yi Ding[1], Tongming Wang[1,2], Virginie Gasciolli[1], Céline Remblière[1], Fabien Marcel[3], Tracy François[3], Abdelhafid Bendahmane[3], Guanghua He[2], Jean Jacques Bono[1] and Benoit Lefebvre[1,#]

[1]LIPME, Université de Toulouse, INRAE, CNRS, Castanet-Tolosan, France

[2]Rice Research Institute, Key Laboratory of Application and Safety Control of Genetically Modified Crops, Academy of Agricultural Sciences, Southwest University, Chongqing 400715, China

[3]Université Paris-Saclay, CNRS, INRAE, Univ Evry, Institute of Plant Sciences Paris-Saclay (IPS2), 91190, Gif sur Yvette, France.

[#]Corresponding author e-mail address: benoit.lefebvre@inrae.fr

Keywords: Arbuscular mycorrhiza, symbiosis, Solanum lycopersicum, Lysin motif receptor like kinases, symbiotic signal perception, Calcium spiking.

Abstract:

Establishment of arbuscular mycorrhiza (AM) relies on a plant signaling pathway that can be activated by fungal chitinic signals such as short chain chitooligosaccharides (CO) and lipo-chitooligosaccharides (LCOs). The tomato LysM receptor-like kinase (LysM RLK) SlLYK10 has high affinity for LCOs and is involved in root colonization by arbuscular mycorrhizal fungi (AMF), however its role in LCO responses has not yet been studied. Here, we show that mutated SlLYK10 proteins produced by *Sllyk10-1* and *Sllyk10-2* mutant alleles, which both cause decreases in AMF colonization, and carry mutations in LysM1 and 2 respectively, have similar LCO binding affinity compared to the WT SlLYK10. However, the mutant forms were not no longer able to induce cell death in *Nicotiana benthamiana* when co-expressed with MtLYK3, a legume LCO co-receptor, while they physically interacted with MtLYK3 in co-purification experiments. This suggests that the LysM mutations affect the ability of SlLYK10 to trigger signaling through a potential co-receptor rather than affect its ability to bind LCOs. Interestingly, tomato lines that contain a calcium (Ca^{2+}) concentration reporter (GECO), showed Ca^{2+} spiking in responses to LCOs, but this occurred only in inner cell layers of the roots, while short chain COs also induced Ca^{2+} spiking in the epidermis. Moreover, the LCO-induced Ca^{2+}spiking was decreased in *Sllyk10-1*GECO* plants, suggesting that the decrease in AMF colonization in *Sllyk10-1* is due to a default in LCO signaling.

Introduction

In terrestrial ecosystems, plants can make symbiotic association with soil microorganisms. Arbuscular mycorrhiza (AM) is an interaction occurring between arbuscular mycorrhizal fungi (AMF) and roots of more than 80% of terrestrial plants (Brundrett and Tedersoo 2018). The fungus receives carbohydrates and lipids from the photosynthetic host (Rich et al. 2017), nutrients essential to complete its life cycle, and provides plants with soil elements, such as nitrogen and phosphate (N and P; Ferrol et al. 2019), which they gather through an extensive mycelium network they develop in the soil. The nutrient exchange mainly occurs in the arbuscules which are highly branched fungal structures formed in the inner root cortex (Bonfante and Genre 2010; Wang et al. 2017).

AM establishment relies on a plant signaling pathway highly conserved among mycotrophic plants, called the common symbiosis signaling pathway (CSSP; Delaux et al. 2014). AMFs produce lipo-chitooligosaccharides (LCOs; Maillet et al. 2011) and short chain chitooligosaccharides (COs, including CO4 and CO5; Genre et al. 2013) considered as responsible for CSSP activation. During plant evolution, the CSSP was recruited for the N-fixing symbiosis in nodulating plants. It was first discovered that LCOs secreted by rhizobia (Nod factors) activate the CSSP leading to calcium (Ca^{2+}) concentration oscillations, known as Ca^{2+} spiking, in and around the nucleus in root hair cells (Ehrhardt, Wais, and Long 1996). Ca^{2+} spiking is now considered as a hallmark of CSSP activation. LCOs and COs were found to induce Ca^{2+} spiking in root epidermal cells of several dicotyledons (Sun et al. 2015; Cope et al. 2019) and monocotyledons (Sun et al. 2015; He et al. 2019, Li et al. 2022).

COs, also called chitin fragment are composed of *N*-acetyl glucosamine (GlcNAc). LCOs differ from short chain CO (CO4/5 consisting in a 4 or 5 GlcNAc linear chain) by an acylation of the terminal non-reducing GlcNAc. Moreover, LCO structural variation, including in the acyl chain length or unsaturation and decorations of the chitinic skeleton such as addition of methyl, fucose, methylfucose, sulfate groups, have been found in LCOs produced by AMF (Maillet et al. 2011; Rush et al. 2020). Although high affinity receptors for short chain COs are not yet known, several high affinity LCO receptors have been identified and belong to various phylogenetic groups of Lysin Motif Receptor-Like Kinases (LysM-RLK; Buendia et al. 2018). Of particular interest, members of the *LYRIA* phylogenetic group in *Medicago truncatula,* (MtNFP)*, Lotus japonicus*, (LjNFR5), or *Solanum lycopersicum*, (SlLYK10)*,* as well as their orthologs in several monocotyledons were shown to be LCO binding receptors (Broghammer et al. 2012; Girardin et al. 2019; Gysel et al. 2021; Cullimore et al., 2023) and essential for the N-fixing symbiosis in most legumes (Radutoiu et al. 2003; Arrighi et al. 2006) and/or involved in AM (Feng et al. 2019; Girardin et al. 2019; He et al., 2019; Li et al. 2022).

LYRIA proteins have an inactive kinase domain. In *M. truncatula* and *L. japonicus*, the LYRIA proteins, MtNFP and LjNFR5, were shown to interact with members of the LysM-RLK *LYKI* phylogenetic group, MtLYK3 and LjNFR1, respectively (Madsen et al. 2011; Moling et al. 2014) that have an active kinase domain. The LYRIA-LYKI receptor complex is thus able to transduce the apoplastic LCO signal in the cell (Buendia et al. 2018). SlLYK10 is a high affinity LCO binding protein and both *SlLYK10* and the LYKI gene *SlLYK12* were shown to be involved in AM establishment in tomato (Girardin et al. 2019; Liao et al. 2018). It is thus likely that these proteins interact to form a LCO receptor complex that controls activation of the CSSP. However, LCO responses have not yet been studied either in tomato or in *Sllyk10* or *Sllyk12* mutants.

We previously reported the mycorrhizal phenotype of the *Sllyk10-1* mutant line. Here we have characterized the impact of amino-acid changes in the proteins encoded by *Sllyk10-1* and by a newly identified allele, *Sllyk10-2*, on their affinity for LCOs and their ability to activate signaling. Moreover, we have characterized Ca^{2+} spiking in response to LCOs and short-chain COs in tomato and found that LCO-induced Ca^{2+} spiking is affected in the *Sllyk10-1* mutant.

Results

The mutations E154K and F88L do not affect SlLYK10 affinity for LCOs

We have previously shown that *SlLYK10* is involved in AM establishment (Girardin et al. 2019). The EMS-mutagenized line *Sllyk10-1* carrying a missense mutation in the sequence encoding the second LysM (E154K, Figure 1(a)) had reduced number of AMF colonization sites, root-length colonization, and expression of AM-marker genes compared with a segregating WT line (Girardin et al. 2019). Here, we have identified another EMS-mutagenized line mutated in *SlLYK10* (*Sllyk10-2*) carrying a missense mutation in the sequence encoding the first LysM (F88L, Figure 1(a)). This line showed a reduction in the number of AMF colonization sites at 3 wpi and in AMF colonization at 4 wpi compared to wild-type (Suppl Figure 1(a-b)), similar to what was observed previously in *Sllyk10-1* (Girardin et al. 2019). The decrease in AMF colonization was similar in the two mutant lines and maintained at 6 wpi (Figure 1(b-c) and Suppl Figure 1(c)).

Since SlLYK10 is an LCO binding protein (Girardin et al. 2019) and we observed a decrease in AMF colonization in *Sllyk10* mutant lines, we hypothesized that these mutations would lead to a decrease in LCO signaling. This could be due to either a lower affinity of the mutated proteins for LCOs and/or lower ability of the mutated proteins to transduce the LCO signal in the cell. To test these hypotheses, we first measured the effect of the mutations on the LCO binding properties of SlLYK10. We previously showed that a chimeric LysM-RLK containing the SlLYK10 extracellular region (ECR),

MtNFP transmembrane domain (TM) and intracellular region (ICR) fused to YFP (thereafter called SlLYK10c-YFP) binds LCO with high affinity, 19 nM ± 4 nM for LCO-V(C18:1,NMe,S) (Girardin et al. 2019). Based on this construction, we used *Agrobacterium tumefaciens*-mediated transient expression to produce chimeras with mutated SlLYK10 ECRs (thereafter called, SlLYK10c^{E154K}-YFP and SlLYK10c^{F88L}-YFP) in leaves of *Nicotiana benthamiana*. Subcellular localization of SlLYK10c^{E154K}-YFP and SlLYK10c^{F88L}-YFP was similar to SlLYK10c-YFP (Figure 2(a)). All proteins were immunodetected in the membrane fractions extracted from *N. benthamiana* leaves (Figure 2(b)). Specific binding of the radiolabeled LCO-V(C18:1,NMe,^{35}S) was significantly increased in membrane fractions from leaves expressing SlLYK10c^{E154K}-YFP, SlLYK10c^{F88L}-YFP, and SlLYK10c-YFP compared to membrane fractions from untransformed leaves (Figure 2(c)), showing that the three proteins are able to bind LCOs. The higher amount of LCO binding in membrane fractions expressing SlLYK10c^{E154K}-YFP is likely due to a higher amount of this protein detected in these membrane fractions compared to the other proteins (Figure 2(b)). As an additional negative control, we tested LCO binding to SlLYK7c:YFP, another tomato LysM-RLK. This protein localization and expression level in *N. benthamiana* leaves is similar to SlLYK10c:YFP (Suppl Figure 2) but the amount of LCO binding in membrane fractions expressing SlLYK7c was similar to that of membrane fractions from untransformed leaves (Figure 2(c)). To characterize in more detail the effect of the mutations on LCO binding properties, we determined the affinity of SlLYK10c^{E154K}-YFP and SlLYK10c^{F88L}-YFP for LCO-V(C18:1,NMe,S) by equilibrium-binding, cold saturation experiments. Scatchard plot analysis revealed a single class of binding sites (Figure 2(d)) with dissociation constants (K_d) of 11 nM ± 2 nM (n=2) and 62 nM ± 27 nM (n=2) for SlLYK10c^{E154K} and SlLYK10c^{F88L} respectively, in the same range of the K_d previously found for SlLYK10c-YFP (19 nM ± 4 nM; Girardin et al. 2019). Together these results suggest that there is no major difference between the mutated proteins and WT SlLYK10 in terms of their affinity for LCO-V(C18:1,NMe,S).

The mutations E154K and F88L might affect ability of SlLYK10 to interact with co-receptors

Since there was no major difference between the mutated and the WT SlLYK10 proteins in their affinity for LCO, we tested the effect of the mutations on the ability of SlLYK10 to interact with putative co-receptors. As a LYR protein, SlLYK10 bears a dead kinase domain, and likely interacts with a LYK protein bearing an active kinase domain (Buendia et al. 2018). Among the tomato LYK genes, *SlLYK12* was shown, as *SlLYK10*, to be involved in AMF colonization, and SlLYK12 has an active kinase domain (Liao et al. 2018), hence is a candidate to form a complex receptor with SlLYK10. We aimed to measure interaction between SlLYK10 and SlLYK12 expressed in *N. benthamiana* leaves.

A. tumefaciens-mediated transient expression of SlLYK12-mTurquoise alone, in *N. benthamiana* leaves, showed expression of the protein in the cell periphery 2 days after *A. tumefaciens* infiltration (dpi, Suppl Figure 3(a)). However, strong necrotic symptoms were observed from 3 dpi (Suppl Figure 3(b)), making impossible to test interaction with *SlLYK10*. Similar necrotic symptoms were induced by expression of the *Arabidopsis thaliana* LYKIA protein AtCERK1-YFP alone in *N. benthamiana* leaves (Pietraszewska-Bogiel et al. 2013). Because necrotic symptoms induced by AtCERK1-YFP were dependent on its kinase activity, we mutated the catalytic residue in the SlLYK12 kinase domain in order to reduce the protein ability to induce necrotic symptoms. SlLYK12^{D437A}-mTurquoise was however still able to induce necrotic symptoms at 3 dpi in *N. benthamiana* leaves (Suppl Figure 3(b)). As an alternative to compare the ability of mutated and WT SlLYK10 proteins to interact with a LYK protein, we used the *M. truncatula* LYKI protein MtLYK3, which was previously shown to induce cell death when co-expressed with the LYRIA MtNFP in *N. benthamiana* leaves, but not when expressed alone (Pietraszewska-Bogiel et al. 2013; Fliegmann et al. 2016). We co-expressed a kinase dead version of MtLYK3 with the various SlLYK10 proteins in *N. benthamiana* leaves. We did not find a decrease in the amount of MtLYK3-HA co-purified with the mutated SlLYK10c-YFP compared to the WT SlLYK10c-YFP (Figure 3(a)). In contrast, co-expression in *N. benthamiana* leaves of WT SlLYK10c-YFP together with an active kinase version of MtLYK3 induced necrotic symptoms, while no visible necrotic symptoms were observed when MtLYK3-mCherry was co-expressed with SlLYK10c^{E154K}-YFP or SlLYK10c^{F88L}-YFP (Suppl Figure 3(c)). The differences in the symptoms induced by the WT and mutated SlLYK10 proteins were even stronger when the proteins were expressed in *Nicotiana tabacum* (Figure 3(b)), a species known to induce stronger cell death responses than *N. benthamiana*. Differences in intensity of necrotic symptoms induced by mutated and WT SlLYK10 proteins co-expressed with MtLYK3 in *N. benthamiana* were confirmed by measuring leaf autofluorescence (Figure 3(c-e)), a way to quantify cell death intensity (Xi et al. 2021).

Altogether, these results suggest that the mutations in SlLYK10 do not affect its affinity for LCO or its ability to interact with a co-receptor, but affect its ability to trigger signaling through a co-receptor.

LCO treatment can activate Ca^{2+} spiking in inner cell layers of tomato roots

There are currently no tools to directly measure LCO responses in tomato. We thus introduced in tomato a nuclear-localized G-GECO (Green Genetically Encoded Ca^{2+} indicators for Optical imaging), a reporter of Ca^{2+} concentrations, to measure Ca^{2+} spiking. We produced *A. tumefaciens* stably transformed lines expressing G-GECO and DsRed. Two independent transgenic lines showing

detectable basal G-GECO fluorescence in the root epidermis (Figure 4(a) and Suppl Figure 4(a)) were selected and multiplied. Plantlets were grown *in vitro* and lateral roots were cut to quantify with a confocal microscope G-GECO fluorescence following chitinic molecule treatments. The DsRed fluorescence was used to verify that nuclei were always in the focal plan during image acquisitions. Since it was previously reported that short chain COs induce Ca^{2+} spiking in non-legume plants, we first tested CO4 at 10^{-7} M. We observed repeated peaks of G-GECO fluorescence in epidermal cells of CO4-treated roots (Figure 4(b)), revealing oscillations in the nuclear Ca^{2+} concentration in response to CO4. In contrast to CO4, none of the LCO structures we tested were able to induce Ca^{2+} spiking in tomato root epidermal cells at 10^{-7} M (Figure 4(c)), even after root pre-treatment with 10^{-7} M 2-aminoethoxyvinyl Gly (AVG) for 2 hours, an inhibitor of ethylene biosynthesis as performed in poplar roots (Cope et al. 2019) to avoid inhibitory effects of ethylene on LCO responses that can occur when plants are grown *in vitro*.

In contrast, we observed Ca^{2+} spiking in response to various LCO structures at 10^{-7} M in inner cell layers of the roots (Figure 4(a, d) and Suppl Figure 4(b)). CO4 also induced Ca^{2+} spiking in these cell layers. No Ca^{2+} spiking was observed when roots were treated with the solvents used for CO4 or LCO stocks (Figure 4(d)). To determine whether inner cell layers of tomato roots show different sensitivities to the various chitinic signal molecules, we quantified the proportion of cells exhibiting Ca^{2+} spiking following the different LCO treatments. All LCO structures tested induced Ca^{2+} spiking. We found that the LCO-IV(C18:1,S) and a mixture of LCO-V bearing fucose or methyl-fucose groups induced Ca^{2+} spiking with the highest cell number (Figure 4(e) and Suppl Figure 4(c)) and were used to compare responses induced by LCOs in WT and *Sllyk10-1*.

Sllyk10-1 shows reduced response to LCOs but not to CO4

In order to test whether LCO responses were affected in *Sllyk10* mutants, we crossed a G-GECO-DsRed line with *Sllyk10-1* and measured, in the progeny, Ca^{2+} spiking following treatment with LCOs or CO4. We found that the proportion of cells exhibiting Ca^{2+} spiking in response to LCOs was significantly reduced in the segregating homozygote plants bearing the *Sllyk10-1* allele compared to the segregating plants bearing the WT *SlLYK10* allele both in root sections (Figure 4(f)) and in intact roots (Suppl Figure 5(a)). Moreover, in the *Sllyk10-1* mutant, in the few cells showing spikes, the frequency of spikes was reduced (Figure 4(g) and Suppl Figure 5(b)). In contrast, similar responses were found in WT and *Sllyk10-1* segregating plants following CO4 treatment both in epidermal and inner cell layers (Figure 4(f) and Suppl Figure 5(b-d)). This result shows that LCO, but not CO4, signaling is affected in *Sllyk10-1*.

Discussion

SlLYK10 is involved in AM establishment

Our previous data showed a reduction in the number of colonization sites in *Sllyk10-1*, which together with expression of the *SlLYK10* promoter in the root epidermis in absence of AMF, suggested a role of *SlLYK10* for AMF penetration in roots (Girardin et al. 2019). Following AMF inoculation, expression of the *SlLYK10* promoter in cortical cells containing developing arbuscules suggested additional roles during the colonization process, particularly for arbuscule formation (Girardin et al. 2019). Here, we found that *Sllyk10-1* and *Sllyk10-2* have both a maintained reduced colonization level by AMF at 4 and 6 wpi, and that all type of AMF structures, hyphae, arbuscules and vesicles, were affected in the two mutant lines.

Mutations in Sllyk10-1 and Sllyk10-2 alleles might affect the ability of the protein to trigger signaling through a co-receptor

The two SlLYK10 residues mutated in proteins encoded by *Sllyk10-1* and *Sllyk10-2* alleles, in LysM2 and LysM1 respectively, have not been characterized in other LYRIA proteins. The mutated residue in the protein produced by the *SlLyk10-1* allele, at position 154, is not far from a residue corresponding to L154 in MtNFP (Figure 5(a)), a critical residue for its role in nodulation and suggested to be involved in LCO binding (Bensmihen et al. 2011; Gysel et al. 2021). The residue 154 in SlLYK10 corresponds to a position where K, E, Q, D are mainly found among the diversity of LYRIA proteins in angiosperms (Gough et al. 2018). No critical residue was previously identified in LysM1 of LYRIA proteins. The mutated residue in the protein produced by the *SlLyk10-2* allele, at position 88, is however very close to a residue corresponding to a residue in the LysM1 of the LYKI protein LjNFR1 that is critical for its role in nodulation (Figure 5(b); Bozsoki et al. 2020). The residue 88 in SlLYK10 corresponds to a position where I, F, V and T, but not L, are mainly found among the diversity of LYRIA protein in angiosperms (Gough et al. 2018).

We did not find strong effect of these mutations on SlLYK10 affinity for LCOs. However, recent data from Gysel et al (2021) suggest that the dynamics of LCO binding (*K*on and *K*off) rather than the affinity (K_d) could be critical for LCO signaling. The LCO binding approach we have used does not permit the determination of *K*on and *K*off. We thus cannot exclude that the two SlLYK10 critical residues modify LCO binding dynamics.

The mutations in SlLYK10 did not affect the ability of SlLYK10 to physically interact with MtLYK3, but affected the ability of SlLYK10 to induce cell death in *N. benthamiana* when co-expressed with MtLYK3. Variable residues in the natural diversity of the LYRIA protein in *Vicia sativa,* VsNFR5, were

suggested to be involved in the interface between VsNFR5 and the LYKI protein, VsK1 (Igolkina et al. 2018). In contrast, the two SlLYK10 critical residues correspond to highly conserved residues (100% identity) in the natural diversity of VsNFR5, consistent with the fact that these residues are not at the LYRIA-LYKI interface and that their mutation does not affect the interaction of SlLYK10 with a LYKI co-receptor. It can be hypothesized that the mutations block signaling through a change of conformation of a SlLYK10-LYKI complex, affecting protein transphosphorylations and/or recruitment in the complex of additional protein(s) required for signaling. Mutations leading to loss of function independently of their ability to bind ligands, have been identified in other RLKs and are proposed to be involved in protein-protein interactions, for example as in the brassinosteroid receptor AtBRI1 (Hothorn et al. 2011). It would, however, need to be verified whether the SlLYK10 mutations affect the interaction of SlLYK10 with SlLYK12 and/or with other potential LYKI interactors in tomato roots.

Distinct LCO and short chain CO receptors are involved in AM

Although LCOs are generally essential for establishment of the nitrogen fixing symbiosis in legumes, the role of LCOs in AM establishment is still not clear, especially now since LCOs were also found to be produced by fungi other than AMF (Cope et al. 2019; Rush et al. 2020). Data that are compatible with a mycorrhizal role of LCOs include the fact that various LCO structures, including structures different from those produced by their specific rhizobial partners, induce Ca^{2+} spiking in the legume and non-legume root epidermis in a CSSP dependent manner (Sun et al. 2015; Li et al. 2022). Our previous data showing that the LYRIA LysM-RLK in tomato and petunia, LYK10, has high affinity for LCOs and plays a role in AM establishment (Girardin et al. 2019) suggested a role of LCO signaling in AM establishment. Here we show that Ca^{2+} spiking, induced by LCOs is affected in an *Sllyk10* mutant line, reinforcing a direct involvement of LCO perception and signaling in AM establishment. Interestingly the LCOs bearing fucose or methylfucose groups that were among those inducing Ca^{2+} spiking in the highest proportion of cells are those found to be the most abundant in AMF (Rush et al. 2020). The fact that short chain COs induced Ca^{2+} spiking similarly in *Sllyk10-1* and WT tomato plants, as found previously in *Mtnfp-2* and WT Medicago plants (Genre et al. 2013), is coherent with specificity of the SlLYK10 LCO binding site for LCOs vs short chain COs (Girardin et al. 2019) and shows that short chain COs are perceived by another as yet uncharacterized receptor.

LCOs might be perceived in the epidermis and transduced to the inner root cell layers by a secondary signal

Although we observed Ca^{2+} spiking in tomato root epidermal cells in response to CO4, no LCO-

induced Ca^{2+} spiking was observed in these cells in our experimental conditions, as first found in rice (Sun et al. 2015). Recent data from Li and co-authors (2022) have demonstrated that LCO-induced Ca^{2+} spiking in the epidermis, in various plant species, depends on nitrogen and phosphorus starvation, and in barley, is associated with an increase in expression of *HvRLK2*, the ortholog of *SlLYK9*. We thus do not exclude that LCOs could induce Ca^{2+} spiking in tomato root epidermal cells in other experimental conditions, but our data clearly show that these cells have a different sensitivity to short chain COs and LCOs.

Surprisingly, LCO-induced Ca^{2+} spiking was observed in deeper tomato root cell layers including at least 3 cell layers surrounding the vascular cylinder, likely comprising the pericycle, the endodermis and the inner cortex, with about a third of the LCO-responding cells being in the cortex and about two-thirds in the root stele (Suppl Figure 4(d)). Responses induced by LCOs in inner root cell layers, including the pericycle, the endodermis and the inner cortex, were also found in legumes, in which cell division, starch accumulation and gene transcription are induced by purified Nod-factors (Ardourel et al. 1994; Truchet et al. 1991, Timmers, et al. 1999, van Zeijl et al. 2015). Another LCO response in inner root cells is the LCO induction of lateral root formation consisting of cell divisions in the pericycle, the endodermis and the inner cortex (Herrbach et al. 2014; Herrbach et al. 2017). In the context of AM, LCO-induced Ca^{2+} spiking in inner root cell layers could be related to similar responses induced at distance by AMF. Indeed, starch accumulation was found in the legume inner root cortex in response to diffusible molecules released by AMF and this was dependent on the CSSP (Gutjahr et al. 2009), and DNA endoreduplication is initiated in the inner root cortex from the early steps of AM development, often at distance from the colonizing AMF hyphae (Carotenuto et al. 2019; Russo et al. 2019). Moreover, LCOs induce lateral root formation in non-legume species (Buendia et al., 2019). Responses in the central cylinder could also be linked to modifications in the stele diameter in mycorrhizal roots (Miller at al., 1997) and in endodermal cell wall depositions expected for nutrient exchanges between arbuscule-containing cells and the vasculature. All these responses might be involved in preparing inner root cell layers for AM.

Symbiotic microbial signals might either be perceived in the epidermis and a secondary signal transduced to inner root cell layers or there could be diffusion from the root surface for perception directly in inner root cell layers. The first hypothesis is supported by data showing that LCO receptors are required in the epidermis but not in the inner root cell layers for nodule organogenesis (Rival et al. 2012; Hayashi et al. 2014) while the latter being initiated by cell divisions in the pericycle, the endodermis and the inner cortex (Xiao et al. 2014). In contrast, decoding of Ca^{2+} spiking is required

both in epidermal and inner root cell layers to trigger cell divisions following root hair colonization by rhizobia (Rival et al. 2012; Hayashi et al. 2014) and for arbuscule formation by AMF (Rival et al. 2013). In tomato, initial LCO perception by the LYRIA protein SlLYK10 might occur in the epidermis, since *SlLYK10* is mainly expressed in the epidermis at a pre-symbiotic stage (Girardin et al. 2019). The subsequent transmission of LCO perception to the inner root cell layers might then be via a secondary signal that would be produced relatively fast since Ca^{2+} spiking was observed about 30 min after LCO treatments.

Materials and Methods

S. lycopersicum mutant identification and genotyping

Induced mutations in the *SlLYK10* gene were isolated as described previously (Clepet et al. 2021) from an ethylmethanesulfonate-mutant population of *Solanum lycopersicum* cv M82 described previously (Piron et al. 2010) and from a new generated collection totaling 10,000 M2 families. The screening was carried out by direct sequencing of target amplicons on a MiSeq system (Illumina) with the primers listed in Suppl Figure 6. The mutation C264A (*Sllyk10-2*) was found in line 1179.

Generation of tomato G-GECO-DsRed lines and cross.

We used *Agrobacterium tumefaciens strain* GV3101 to introduce a NLS-G-GECO and DsRed construct (Cope et al. 2019) in the M82 tomato cultivar with the cotyledon transformation method described in (Van Eck et al. 2019). Transgenic diploid T0 plants were selected using 150mg/L Kanamycin and flow cytometry. Among the latter, we selected 2 lines based on their level of basal G-GECO fluorescence. T1 G-GECO-DsRed plants were crossed with *Sllyk10-1* plants (Girardin et al. 2019). F1 and F2 plants were genotyped by sequencing (Sanger) a similar amplicon that the one described above, for *Sllyk10-1*, and by basal fluorescence for presence of the G-GECO construct.

Cloning

SlLYK10c-YFP construct is from (Girardin et al. 2019). For the SlLYK10c^{E154K}-YFP and SlLYK10c^{F88L}-YFP constructs, we used site-directed mutagenesis (primers are listed in Suppl Figure 6) to introduce the mutations of G460A and C264A on the sequence coding SlLYK10 extracellular region (ECR) coding sequence. The sequence coding the SlLYK7 ECR (Solyc02g089920) was amplified by PCR (primers are listed in Suppl Figure 6). The sequences coding mutated SlLYK10 ECR and SlLYK7 ECR were cloned in translational fusion with the sequences encoding the TM/ICR of MtNFP and YFP under the control of *Pro35S* in a pCambia 2200 vector modified for golden gate cloning as for *SlLYK10c*. *SlLYK12* (Solyc02g081050) coding sequence (Suppl Figure 7) was produced by gene synthesis, then cloned in translational fusion with the sequence coding mTurquoise under the control of *Pro35S* in a pCambia

2200 vector modified for golden gate cloning. For the SlLYK12^{D437A} construct, we used site-directed mutagenesis (primers are listed in Suppl Figure 6) to introduce the mutation of A1310C into the sequence coding SlLYK12 kinase domain and cloned as for SlLYK12-mTurquoise construct. All constructs were introduced in *Agrobacterium tumefaciens* LBA4404 VirGN54D. The MtLYK3-mcherry construct is from (Pietraszewska-Bogiel et al. 2013). The sequence coding for MtLYK3^{G334E} was cloned in translational fusion with the HA-tag under the control of *Pro35S* in a pCambia 2200 vector modified for golden gate cloning. All constructs were verified by Sanger sequencing.

AM phenotyping

Tomato seeds were surface sterilized and germinated in sterile water. Tomato plantlets were then transferred in 50 ml containers (one plantlet / container) filled with attapulgite (Oil Dri UK), watered with 20 ml of 0.5x modified Long ashton (7.5 µM NaH_2PO_4), and inoculated with 500 spores of *Rhizophagus irregularis* DAOM 197198 (Agronutrition). Roots were harvested at 4 or 6 weeks post inoculation, washed and stained using an ink-vinegar solution.

Transient Expression in N. benthamiana

For LCO binding assays, subcellular localization, co-immunopurification and necrotic symptom analysis, 4-week-old *N. benthamiana* leaves were fully infiltrated with *A. tumefaciens* LBA4404 virGN54D strain containing the expression vectors. *A. tumefaciens* strains were grown overnight at 28°C in liquid LB medium supplemented with appropriate antibiotics. Bacteria were washed and diluted in 10 mM MES, pH 5.6, 10mM MgCl2, and 100 µM acetosyringone. The p19 protein, which inhibits gene silencing was co-expressed with the proteins of interest.

LCO binding assays

Approximately 10 g of leaves were homogenized at 4°C in a blender in the presence of 20 ml of extraction buffer (25 mM Tris, pH 8.5, 0.47 M sucrose, 5 mM EDTA, 10 mM DTT, 0.6% PVPP and protease inhibitors). Samples were centrifuged for 15 min at 3000 *g*, and then the supernatant was recentrifuged for 30 min at 80 000 *g*. The pellet (membrane fraction) was first washed in 5 ml and then resuspended in 2 ml of binding buffer (25 mM Na-Cacodylate pH 6, 250 mM sucrose, 1 mM CaCl2, 1 mM MgCl2 and protease inhibitors). The amount of fusion proteins was quantified by immunoblotting of 10 µg of membrane fraction proteins using anti-GFP antibodies.

PAPS was synthesized in the presence of 500 µCi of ^{35}S sodium sulfate and yeast extract, and used as a substrate for a sulfotransferase to introduce ^{35}S on LCO-V(C18:1,NMe). LCO binding assays were performed with membrane fractions containing 20 µg of proteins, 1 nM of LCO-V(C18:1,NMe,^{35}S) and a range of unlabeled LCO-V(C18:1,NMe,S) from 1 nM to 1 µM. Incubations were performed for

1 h in 96-well microtiter plates on ice, and then filtered and washed. Radioactivity (DPM) in the membrane fractions was measured with a scintillation counter. Incubation of the membrane fractions with the radiolabeled ligand, LCO-V(C18:1,NMe,^{35}S), in the absence or in the presence of 1 µM unlabeled LCO-V(C18:1,NMe,S) allowed to determine the total and non-specific binding respectively and by difference the specific binding.

LCO binding assays were performed independently on the mutated SlLYK10c proteins and the SlLYK7c protein, each with the positive (WT SlLYK10c) and negative (untransformed) controls. All data were pooled in Figure 2(c).

Co-immunopurification

N. benthamiana leaves were crushed in liquid nitrogen and proteins solubilized for 30 min at 4 °C in IP buffer (25 mM HEPES pH7.5, 150 mM NaCl, 10% glycerol, 10 mM EDTA, 1 mM DTT, phosphatase and protease inhibitors) containing 0.2 % dodecyl-maltoside (DDM), with a ratio 1:4 (w:v). Supernatant (solubilized fraction) after a 20 min centrifugation at 100 000 *g* was diluted twice in IP buffer and incubated with 10 µl of washed magnetic agarose beads coupled to anti-GFP nanobodies (Chromotek) for 2 h at 4°C. Beads were washed three times with IP buffer containing 0.1 % DDM and proteins were eluted in 50 µL of 2X Laemmli buffer at 95°C for 5 min.

Short chain CO/LCO treatments

A segregating F2 G-GECO-DsRed**Sllyk10-1* population was used. Individual plants were genotyped to identify homozygote *Sllyk10-1* and WT SlLYK10 plants and the presence of the G-GECO-DsRed construct. Plantlets were grown on agar supplemented with 25mg/L kanamycin for 6 weeks. About 2 cm long root pieces corresponding to middle parts of the secondary roots were cut and put between glass slides and treated with approximately 200µl 10^{-7}M LCO or for CO4 30min before microscopy analysis. As LCO stocks (10^{-4} M) were in 50% ethanol, we treated controls with 0.05% ethanol. The synthetic LCO-IV(C16:0,S), LCO-IV(C16:0), LCO-IV(C18:1,S), LCO-IV(C18:1) are as in Maillet et al, 2021, the mixture of synthetic LCO-V(C18:1,Fuc)/LCO-V(C18:1,MeFuc) is as in (Bonhomme et al. 2021), the natural LCO-V(C18:1,NMe,S) and LCO-V(C18:1,NMe) were purified from the rhizobial strain *Rhizobium tropici*. CO4 (Megazyme) stock was 10^{-4} M in water.

Microscopy analyses

All image were acquired using a SP8 confocal laser-scanning microscope (Leica) with a fluotar VISIR 25x/0.95 WATER objective. For subcellular localization, YFP and m-turquoise were respectively excited with the 488-nm line of an argon laser or 448-nm, and emissions (520 to 555 nm or 455 to 600 nm) were imaged. For cell death quantification, auto-fluorescence was excited with the 405-

nm line of an argon laser and fluorescent emissions (415 to 506 nm) were measured in randomly pick-up leaf discs. The images were acquired with a scanning resolution of 1024 ×1024 pixels. Settings (laser intensity, gain, offset, magnification, airy units) were similar between observations for all samples. After acquiring images, we used Image J to measure the mean fluorescence intensity in each image. For Ca^{2+} spiking measurement G-GECO and DsRed were respectively excited with the 488-nm or the 561-nm argon laser lines, and fluorescent emission (500 to 550 nm or 570 to 650 nm) were imaged. Images were acquired at 6.29s intervals with a scanning resolution of 512×512 pixels. Settings (laser intensity, gain, offset, magnification, airy units) were similar between observations for all samples. Following 20min captures, all nuclei in the focal plan were designated as specific regions of interest using the software LAS X (version 3.3), and the fluorescence intensities in each region of interest were exported. Total number of cells with visible G-GECO basal fluorescence and the number of cells with nuclei spiking more than once were used to calculate the percentage of cells with spiking nuclei.

Data and material availability

All data, plant lines and constructs are available upon request.

Acknowledgments: We thank Sylvian Cottaz and Sebastien Fort (CERMAV) for LCO synthesis and Fabienne Maillet (LIPME) for purification of rhizobial LCOs. We thank Julie Cullimore, Clare Gough and Sandra Bensmihen for critical reading of the manuscript. We thank Wu Xi Shu Guang Agricultural Science and Technology Development Co. Ltd. for a PhD fellowship for Yi Ding. This work was supported by the ANR project “WHEATSYM” (ANR-16-CE20-0025-01), the National Natural Science Foundation of China (Grant No. 32100241) and the Foundation for Innovative Research Groups of the Natural Science Foundation of Chongqing (Grant No. cstc2021jcyj-cxttx0004). This study is set within the framework of the "Laboratoires d’Excellences (LABEX)" TULIP (ANR-10-LABX-41), SPS (ANR-10-LABX-40-SPS) and of the "École Universitaire de Recherche (EUR)" TULIP-GS (ANR-18-EURE-0019). The authors declare no conflicts of interest.

Author Contributions

B.L designed research; Y.D., T.W., V.G., C.R, F.M. and T.F. performed research; A.B., G.H., J.J.B, and B.L analyzed data. B.L. wrote the paper.

Disclosures

The authors have no conflicts of interest to declare.

References:

Ardourel, M., N. Demont, F. D. Debelle, F. Maillet, F. Debilly, J. C. Prome, J. Denarie, and G. Truchet. 1994. Rhizobium Meliloti Lipooligosaccharide Nodulation Factors - Different Structural Requirements for Bacterial Entry into Target Root Hair-Cells and Induction of Plant Symbiotic Developmental Responses. Plant Cell 6 :1357-1374.

Arrighi, J. F., A. Barre, B. Ben Amor, A. Bersoult, L. C. Soriano, R. Mirabella, F. de Carvalho-Niebel, E. P. Journet, M. Ghérardi, T. Huguet, R. Geurts, J. Dénarié, P. Rougé, and C. Gough. 2006. The Medicago truncatula lysin motif-receptor-like kinase gene family includes NFP and new nodule-expressed genes. Plant Physiol 142 :265-79.

Bensmihen, S., F. de Billy, and C. Gough. 2011. Contribution of NFP LysM domains to the recognition of Nod factors during the Medicago truncatula/Sinorhizobium meliloti symbiosis. PLoS One 6 :e26114.

Bonfante, P., and A. Genre. 2010. Mechanisms underlying beneficial plant-fungus interactions in mycorrhizal symbiosis. Nat Commun 1:48.

Bonhomme, M., S. Bensmihen, O. André, E. Amblard, M. Garcia, F. Maillet, V. Puech-Pagès, C. Gough, S. Fort, S. Cottaz, G. Bécard, and C. Jacquet. 2021. Distinct genetic basis for root responses to lipo-chitooligosaccharide signal molecules from different microbial origins. J Exp Bot 72 :3821-3834.

Bozsoki, Z., K. Gysel, S. B. Hansen, D. Lironi, C. Krönauer, F. Feng, N. de Jong, M. Vinther, M. Kamble, M. B. Thygesen, E. Engholm, C. Kofoed, S. Fort, J. T. Sullivan, C. W. Ronson, K. J. Jensen, M. Blaise, G. Oldroyd, J. Stougaard, K. R. Andersen, and S. Radutoiu. 2020. Ligand-recognizing motifs in plant LysM receptors are major determinants of specificity. Science 369 :663-670.

Broghammer, A., L. Krusell, M. Blaise, J. Sauer, J. T. Sullivan, N. Maolanon, M. Vinther, A. Lorentzen, E. B. Madsen, K. J. Jensen, P. Roepstorff, S. Thirup, C. W. Ronson, M. B. Thygesen, and J. Stougaard. 2012. Legume receptors perceive the rhizobial lipochitin oligosaccharide signal molecules by direct binding. Proc Natl Acad Sci USA 109 :13859-64.

Brundrett, M. C., and L. Tedersoo. 2018. Evolutionary history of mycorrhizal symbioses and global host plant diversity. New Phytol 220:1108-1115.

Buendia, L., A. Girardin, T. Wang, L. Cottret, and B. Lefebvre. 2018. LysM Receptor-Like Kinase and LysM Receptor-Like Protein Families: An Update on Phylogeny and Functional Characterization. Front Plant Sci 9:1531.

Buendia, L., Maillet, F., O'Connor, D., van de-Kerkhove, Q., Danoun, S., Gough, C., Lefebvre, B. and Bensmihen, S. 2019. Lipo-chitooligosaccharides promote lateral root formation and modify auxin homeostasis in Brachypodium distachyon. New Phytol, 221, 2190-2202.Carotenuto, G., V. Volpe, G. Russo, M. Politi, I. Sciascia, J. de Almeida-Engler, and A. Genre. 2019. Local endoreduplication as a feature of intracellular fungal accommodation in arbuscular mycorrhizas. New Phytol 223 :430-446.

Clepet C, R. S. Devani, R. Boumlik, Y. Hao, H. Morin, F. Marcel, M. Verdenaud, B. Mania, G. Brisou, S. Citerne, G. Mouille, J. C. Lepeltier, S. Koussevitzky, A. Boualem, A. Bendahmane. 2021. The miR166-SlHB15A regulatory module controls ovule development and parthenocarpic fruit set under adverse temperatures in tomato. Mol Plant 14:1185-1198.

Cope, K. R., A. Bascaules, T. B. Irving, M. Venkateshwaran, J. Maeda, K. Garcia, T. A. Rush, C. Ma, J. Labbé, S. Jawdy, E. Steigerwald, J. Setzke, E. Fung, K. G. Schnell, Y. Wang, N. Schlief, H. Bücking, S. H. Strauss, F. Maillet, P. Jargeat, G. Bécard, V. Puech-Pagès, and J. M. Ané. 2019. The Ectomycorrhizal Fungus Laccaria bicolor Produces Lipochitooligosaccharides and Uses the Common Symbiosis Pathway to Colonize Populus Roots. Plant Cell 31 :2386-2410.

Delaux, PM, K Varala, PP Edger, GM Coruzzi, JC Pires, and JM Ane. 2014. Comparative Phylogenomics Uncovers the Impact of Symbiotic Associations on Host Genome Evolution. Plos Genet 10 :e1004487.

Ehrhardt, D. W., R. Wais, and S. R. Long. 1996. Calcium spiking in plant root hairs responding to Rhizobium nodulation signals. Cell 85 :673-681.

Feng, F., J. Sun, G. V. Radhakrishnan, T. Lee, Z. Bozsóki, S. Fort, A. Gavrin, K. Gysel, M. B. Thygesen, K. R. Andersen, S. Radutoiu, J. Stougaard, and G. E. D. Oldroyd. 2019. A combination of chitooligosaccharide and lipochitooligosaccharide recognition promotes arbuscular mycorrhizal associations in Medicago truncatula. Nat Commun 10 :5047.

Ferrol, N., C. Azcón-Aguilar, and J. Pérez-Tienda. 2019. Review: Arbuscular mycorrhizas as key players in sustainable plant phosphorus acquisition: An overview on the mechanisms involved. Plant Sci 280:441-447.

Fliegmann, J., A. Jauneau, C. Pichereaux, C. Rosenberg, V. Gasciolli, A. C. Timmers, O. Burlet-Schiltz, J. Cullimore, and J. J. Bono. 2016. LYR3, a high-affinity LCO-binding protein of Medicago truncatula, interacts with LYK3, a key symbiotic receptor. FEBS Lett 590 :1477-87.

Genre, A., M. Chabaud, C. Balzergue, V. Puech-Pages, M. Novero, T. Rey, J. Fournier, S. Rochange, G. Becard, P. Bonfante, and D. G. Barker. 2013. Short-chain chitin oligomers from arbuscular mycorrhizal fungi trigger nuclear Ca2+ spiking in Medicago truncatula roots and their production is enhanced by strigolactone. New Phytol 198 :179-189.

Girardin, A., T. Wang, Y. Ding, J. Keller, L. Buendia, M. Gaston, C. Ribeyre, V. Gasciolli, M. C. Auriac, T. Vernié, A. Bendahmane, M. K. Ried, M. Parniske, P. Morel, M. Vandenbussche, M. Schorderet, D. Reinhardt, P. M. Delaux, J. J. Bono, and B. Lefebvre. 2019. LCO Receptors Involved in Arbuscular Mycorrhiza Are Functional for Rhizobia Perception in Legumes. Curr Biol 29 :4249-4259.

Gough, C., L. Cottret, B. Lefebvre, and J. J. Bono. 2018. Evolutionary History of Plant LysM Receptor Proteins Related to Root Endosymbiosis. Front Plant Sci 9:923.

Gutjahr, C., M. Novero, M. Guether, O. Montanari, M. Udvardi, and P. Bonfante. 2009. Presymbiotic factors released by the arbuscular mycorrhizal fungus Gigaspora margarita induce starch accumulation in Lotus japonicus roots. New Phytol 183 :53-61.

Gysel, K., M. Laursen, M. B. Thygesen, D. Lironi, Z. Bozsóki, C. T. Hjuler, N. N. Maolanon, J. Cheng, P. K. Bjørk, M. Vinther, L. H. Madsen, H. Rübsam, A. Muszyński, A. Ghodrati, P. Azadi, J. T. Sullivan, C. W. Ronson, K. J. Jensen, M. Blaise, S. Radutoiu, J. Stougaard, and K. R. Andersen. 2021. Kinetic proofreading of lipochitooligosaccharides determines signal activation of symbiotic plant receptors. Proc Natl Acad Sci USA 118 :e2111031118.

Hayashi, T., Y. Shimoda, S. Sato, S. Tabata, H. Imaizumi-Anraku, and M. Hayashi. 2014. Rhizobial infection does not require cortical expression of upstream common symbiosis genes responsible for the induction of Ca2+ spiking. Plant Journal 77 :146-159.

He, J., Zhang, C., Dai, H., Liu, H., Zhang, X., Yang, J., Chen, X., Zhu, Y., Wang, D., Qi, X., Li, W., Wang, Z., An, G., Yu, N., He, Z., Wang, Y.F., Xiao, Y., Zhang, P. and Wang, E. 2019. A LysM Receptor Heteromer Mediates Perception of Arbuscular Mycorrhizal Symbiotic Signal in Rice. Mol Plant, 12, 1561–1576.

Herrbach, V., Remblière, C., Gough, C. and Bensmihen, S. 2014. Lateral root formation and patterning in Medicago truncatula. J Plant Physiol, 171, 301-310.

Herrbach, V., Chirinos, X., Rengel, D., Agbevenou, K., Vincent, R., Pateyron, S., Huguet, S., Balzergue, S., Pasha, A., Provart, N., Gough, C. and Bensmihen, S. 2017. Nod factors potentiate auxin signaling for transcriptional regulation and lateral root formation in Medicago truncatula. J Exp Bot, 68, 569-583.

Hothorn, M., Y. Belkhadir, M. Dreux, T. Dabi, J. P. Noel, I. A. Wilson, and J. Chory. 2011. Structural basis of steroid hormone perception by the receptor kinase BRI1. Nature 474 :467-71.

Igolkina, A. A., Y. B. Porozov, E. P. Chizhevskaya, and E. E. Andronov. 2018. Structural Insight Into the Role of Mutual Polymorphism and Conservatism in the Contact Zone of the NFR5-K1 Heterodimer With the Nod Factor. Front Plant Sci 9 :344.

Li, X.R., Sun, J., Albinsky, D., Zarrabian, D., Hull, R., Lee, T., Jarratt-Barnham, E., Chiu, C.H., Jacobsen, A., Soumpourou, E., Albanese, A., Kohlen, W., Luginbuehl, L.H., Guillotin, B., Lawrensen, T., Lin, H., Murray, J., Wallington, E., Harwood, W., Choi, J., Paszkowski, U. and Oldroyd, G.E.D. 2022. Nutrient regulation of lipochitooligosaccharide recognition in plants via NSP1 and NSP2. Nat Commun, 13, 6421.

Liao, DH, X Sun, N Wang, FM Song, and Y Liang. 2018. Tomato LysM Receptor-Like Kinase SlLYK12 Is Involved in Arbuscular Mycorrhizal Symbiosis. Front Plant Sci 9 :1004

Madsen, E. B., M. Antolín-Llovera, C. Grossmann, J. Ye, S. Vieweg, A. Broghammer, L. Krusell, S. Radutoiu, O. N. Jensen, J. Stougaard, and M. Parniske. 2011. Autophosphorylation is essential for the in vivo function of the Lotus japonicus Nod factor receptor 1 and receptor-mediated signalling in cooperation with Nod factor receptor 5. Plant J 65 :404-17.

Maillet, F., V. Poinsot, O. André, V. Puech-Pagès, A. Haouy, M. Gueunier, L. Cromer, D. Giraudet, D. Formey, A. Niebel, E. A. Martinez, H. Driguez, G. Bécard, and J. Dénarié. 2011. Fungal lipochitooligosaccharide symbiotic signals in arbuscular mycorrhiza. Nature 469 :58-63.

Miller, R., Hetrick, B. and Wilson, G. 1997 Mycorrhizal fungi affect root stele tissue in grasses. Canadian Journal of Botany, 75, 1778-1784.

Moling, S., A. Pietraszewska-Bogiel, M. Postma, E. Fedorova, M. A. Hink, E. Limpens, T. W. Gadella, and T. Bisseling. 2014. Nod factor receptors form heteromeric complexes and are essential for intracellular infection in medicago nodules. Plant Cell 26 :4188-99.

Pietraszewska-Bogiel, Anna, Benoit Lefebvre, Maria A. Koini, Doerte Klaus-Heisen, Frank L. W. Takken, Rene Geurts, Julie V. Cullimore, and Theodorus W. J. Gadella. 2013. Interaction of Medicago truncatula Lysin Motif Receptor-Like Kinases, NFP and LYK3, Produced in Nicotiana benthamiana Induces Defence- Like Responses. Plos One 8 :e65055.

Piron, F., M. Nicolaï, S. Minoïa, E. Piednoir, A. Moretti, A. Salgues, D. Zamir, C. Caranta, and A. Bendahmane. 2010. An induced mutation in tomato eIF4E leads to immunity to two potyviruses. PLoS One 5 :e11313.

Radutoiu, S., L. H. Madsen, E. B. Madsen, H. H. Felle, Y. Umehara, M. Gronlund, S. Sato, Y. Nakamura, S. Tabata, N. Sandal, and J. Stougaard. 2003. Plant recognition of symbiotic bacteria requires two LysM receptor-like kinases. Nature 425 :585-92.

Rich, M. K., E. Nouri, P. E. Courty, and D. Reinhardt. 2017. Diet of Arbuscular Mycorrhizal Fungi: Bread and Butter? Trends Plant Sci 22 :652-660.

Rival, P., F. de Billy, J. J. Bono, C. Gough, C. Rosenberg, and S. Bensmihen. 2012. Epidermal and cortical roles of NFP and DMI3 in coordinating early steps of nodulation in Medicago truncatula. Development 139 :3383-91.

Rival, P., Bono, J.J., Gough, C., Bensmihen, S. and Rosenberg, C. 2013. Cell autonomous and non-cell autonomous control of rhizobial and mycorrhizal infection in Medicago truncatula. Plant Signal Behav, 8, e22999.Rush, T. A., V. Puech-Pagès, A. Bascaules, P. Jargeat, F. Maillet, A. Haouy, A. Q. Maës, C. C. Carriel, D. Khokhani, M. Keller-Pearson, J. Tannous, K. R. Cope, K. Garcia, J. Maeda, C. Johnson, B. Kleven, Q. J. Choudhury, J. Labbé, C. Swift, M. A. O'Malley, J. W. Bok, S. Cottaz, S. Fort, V. Poinsot, M. R. Sussman, C. Lefort, J. Nett, N. P. Keller, G. Bécard, and J. M. Ané. 2020. Lipo-chitooligosaccharides as regulatory signals of fungal growth and development. Nat Commun 11

:3897.

Russo, G., G. Carotenuto, V. Fiorilli, V. Volpe, M. Chiapello, D. Van Damme, and A. Genre. 2019. Ectopic activation of cortical cell division during the accommodation of arbuscular mycorrhizal fungi. New Phytol 221 :1036-1048.

Sun, J., J. B. Miller, E. Granqvist, A. Wiley-Kalil, E. Gobbato, F. Maillet, S. Cottaz, E. Samain, M. Venkateshwaran, S. Fort, R. J. Morris, J. M. Ané, J. Dénarié, and G. E. Oldroyd. 2015. Activation of symbiosis signaling by arbuscular mycorrhizal fungi in legumes and rice. Plant Cell 27 :823-38.

Timmers, A. C., M. C. Auriac, and G. Truchet. 1999. Refined analysis of early symbiotic steps of the Rhizobium-Medicago interaction in relationship with microtubular cytoskeleton rearrangements. Development 126 :3617-3628.

Truchet, G., P. Roche, P. Lerouge, J. Vasse, S. Camut, F. de Billy, JC. Prome, and J. Dénarié. 1991. Sulphated lipo-oligosaccharide signals of Rhizobium meliloti elicit root nodule organogenesis in alfalfa. Nature 351 :670-673.

Van Eck, J., P. Keen, and M. Tjahjadi. 2019. Agrobacterium tumefaciens-Mediated Transformation of Tomato. In Transgenic Plants. Methods in Molecular Biology,, edited by S. Kumar, P. Barone and M. Smith, 225-234. Humana Press, New York.

van Zeijl, A., Op den Camp, R.H., Deinum, E.E., Charnikhova, T., Franssen, H., Op den Camp, H.J., Bouwmeester, H., Kohlen, W., Bisseling, T. and Geurts, R. 2015. Rhizobium Lipo-chitooligosaccharide Signaling Triggers Accumulation of Cytokinins in Medicago truncatula Roots. Mol Plant, 8, 1213-1226.

Wang, W., J. Shi, Q. Xie, Y. Jiang, N. Yu, and E. Wang. 2017. Nutrient Exchange and Regulation in Arbuscular Mycorrhizal Symbiosis. Mol Plant 10 :1147-1158.

Xi, Y., V. Chochois, T. Kroj, and S. Cesari. 2021. A novel robust and high-throughput method to measure cell death in Nicotiana benthamiana leaves by fluorescence imaging. Mol Plant Pathol 22 :1688-1696.

Xiao, T. T., S. Schilderink, S. Moling, E. E. Deinum, E. Kondorosi, H. Franssen, O. Kulikova, A. Niebel, and T. Bisseling. 2014. Fate map of Medicago truncatula root nodules. Development 141 :3517-28.

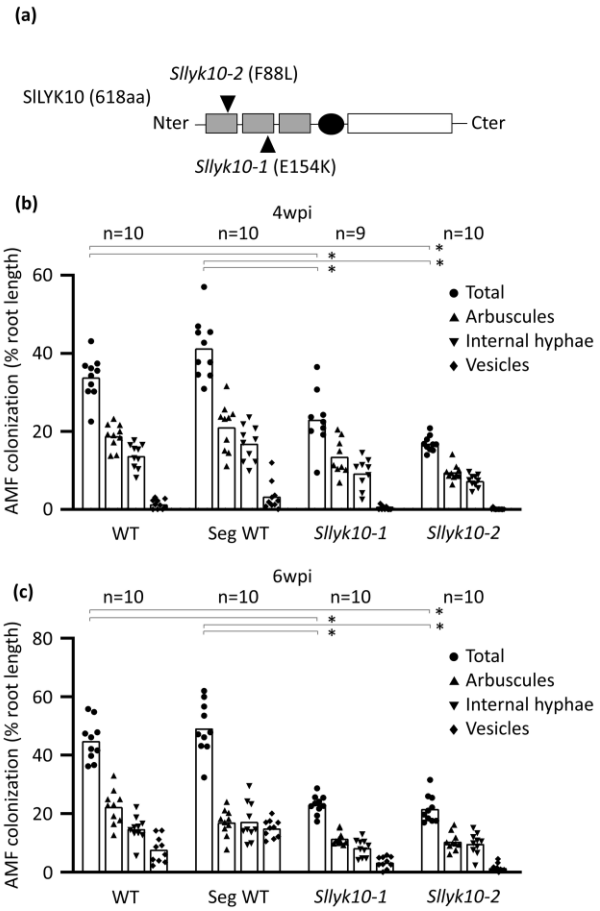

Figure 1. *Sllyk10-2* is affected in AMF colonization

(a) Position of F88L and E154K point mutations on the SlLYK10 schematic structure. Grey: LysM, Black: transmembrane domain, White: kinase domain. (b-c) Detailed analysis of AMF structures found in WT plants (WT), segregating progenies of mutagenized lines bearing the WT *SlLYK10* allele (seg WT), the *Sllyk10-1* allele (*Sllyk10-1*), or the *Sllyk10-2* allele (*Sllyk10-2)* harvested at 4 wpi (b) or 6 wpi (c). Individual samples and means between the indicated numbers of root systems obtained from 1 experiment, are shown. Statistical differences (* p-value < 0.05) were calculated using a Kruskal Wallis test and detailed results are shown in Suppl Figure 1(c).

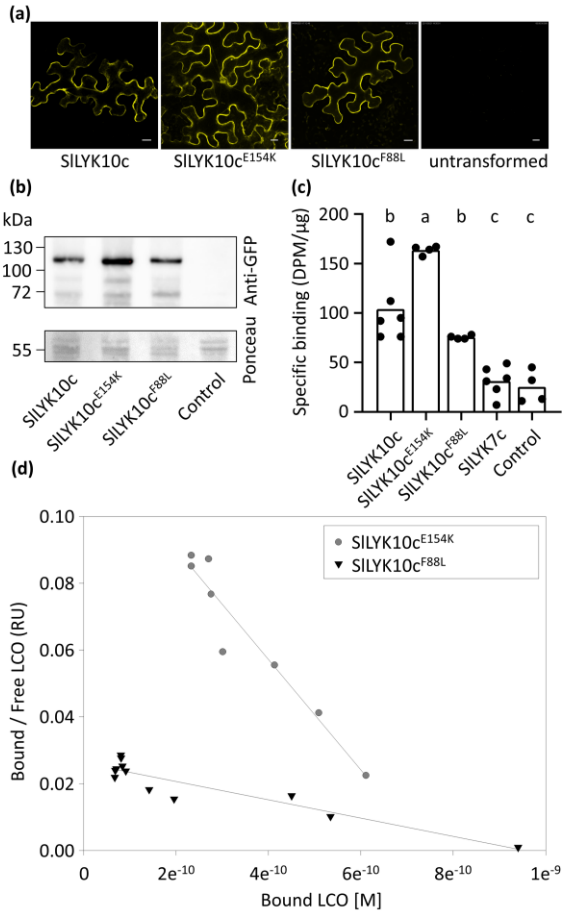

Figure 2. SlLYK10c^{E154K} and SlLYK10c^{F88L} bind LCO as WT SlLYK10

(a) Confocal images of epidermal cells from *N. benthamiana* leaves expressing the indicated proteins tagged with YFP. Scale bars represent 20µm. (b) Immunodetection with anti YFP antibodies in 10µg of membrane fractions from *N. benthamiana* leaves expressing the indicated YFP-tagged proteins. The ponceau red staining shows the protein loading. (c) Specific binding of LCO-V(C18:1,NMe,^{35}S) to membrane fractions containing the indicated proteins expressed as amount of radioactivity (disintegrations per minute, DPM) per quantity of proteins in the membrane fractions. Bar plot shows the individual samples and means between at least two technical replicates on two independent batches of membrane fractions (n≥4). Different letters mean significant difference using a pairwise T-test. (d) Scatchard plots of cold saturation experiments using the indicated proteins and a range of LCO-V(C18:1,NMe,S) concentrations as competitor. The plots are representative of experiments performed with two independent batches of membrane fractions.

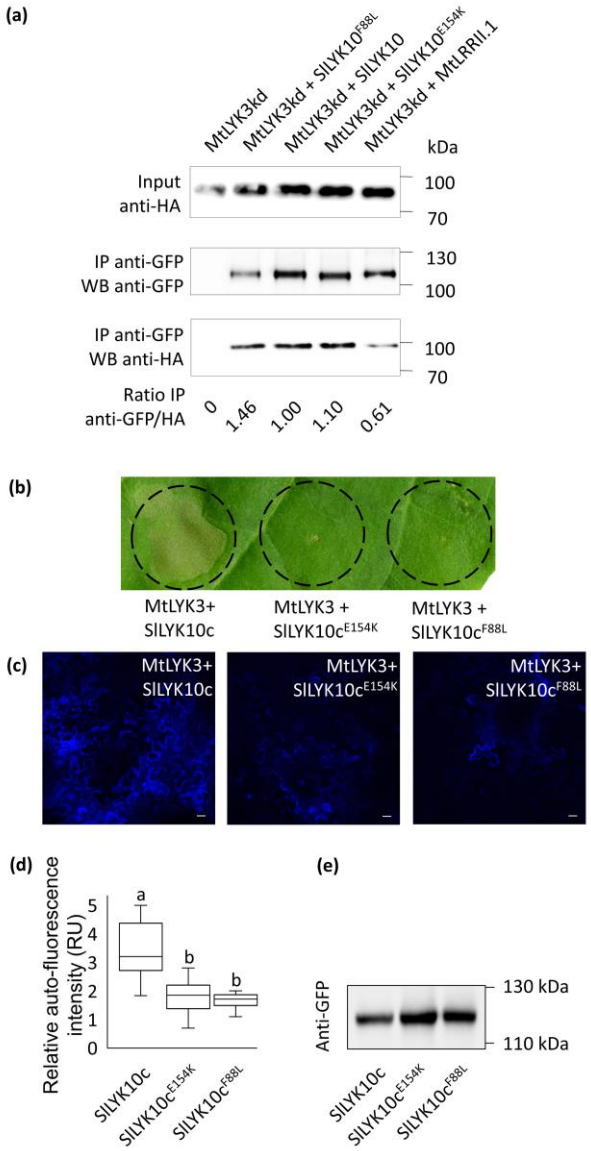

Figure 3. Co-expression of MtLYK3 with WT SlLYK10c, but not with SlLYK10c^{E154K} and SlLYK10c^{F88L} induces necrotic symptoms in *N*. *benthamiana* leaves.

(a) Co-purification of MtLYK3^{G334E}-HA with SlLYK10c-YFP, SlLYK10c^{E154K}-YFP and SlLYK10c^{F88L}-YFP. Solubilized proteins from *N*. *benthamiana* leaves expressing the indicated proteins were purified using anti-GFP beads (IP). Purified proteins were detected using anti-GFP antibodies (WB anti-GFP) and co-purified proteins using anti-HA antibodies (WB anti-HA). Ratios between the intensity of the bands corresponding to YFP and HA fusion proteins are indicated below. Note that part of LYK3 co-purification is nonspecific since also found with the negative control MtLRII.1-YFP. Similar results were obtained in an independent experiment. (b) Representative images of adaxial sides of *N*. *tabacum* leaves expressing the indicated proteins at 3 dpi. (c) Representative confocal images of autofluorescence observed at 3 dpi in abaxial side of *N*. *benthamiana* leaves co-expressing MtLYK3 and the indicated proteins. (d) Quantification of the autofluorescence induced by co-expression of MtLYK3 and the indicated proteins. Box plots represent the level of autofluorescence at 3 dpi in at least 25 samples obtained from 3 independent experiments. Values are normalized by the level of autofluorescence in untransformed leaves. Different letters mean significant differences using a Kruskal Wallis test on the total number of samples analyzed. (e) Immunodetection of the YFP-fusion proteins in total extract of leaves expressing the indicated proteins in absence of MtLYK3-mCherry.

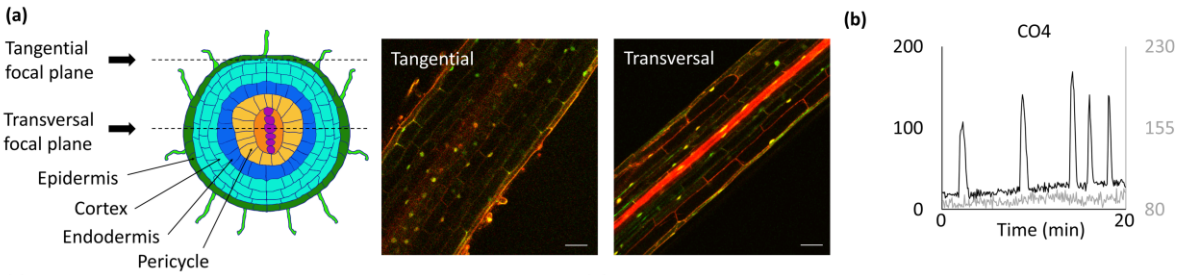

(c)

Treatment	Responding epidermal cells
Control	0/80
LCO-IV(C16:0)	0/107
LCO-IV(C18:1)	0/87
LCO-V(C18:1,NMe)	0/38
LCO-IV(C18:1,S)	0/57
LCO-V(C18:1,Fuc/MeFuc)	0/87
CO4	12/41 (**29.3%**)

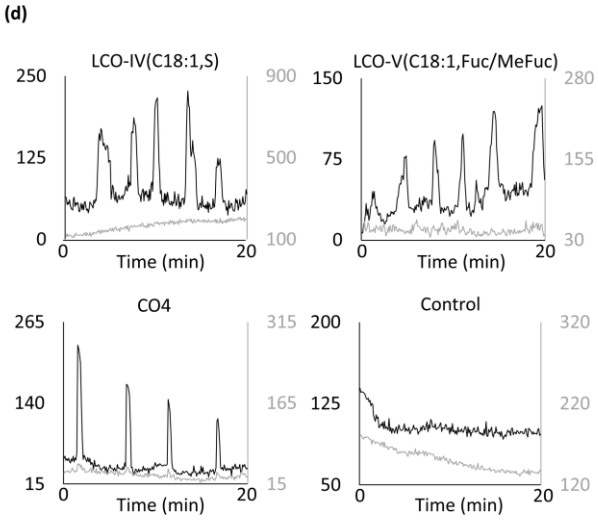

(e)

Treatment	Responding inner layer cells
Control	0/59
LCO-IV(C16:0)	23/157 (**14.6%**)
LCO-IV(C18:1)	21/188 (**11.6%**)
LCO-V(C18:1,NMe)	12/82 (**14.6%**)
LCO-IV(C16:0,S)	14/96 (**14.6%**)
LCO-IV(C18:1,S)	18/64 (**28.1%**)
LCO-V(C18:1,NMe,S)	17/119 (**14.3%**)
LCO-V(C18:1,Fuc/MeFuc)	36/106 (**34.0%**)
CO4	9/47 (**19.1%**)

(f)

Treatment	Responding inner layer cells	
	Seg WT	*Sllyk10-1*
CO4	30/98 (**30.6%**)	28/103 (**27.2%**)
LCO-IV (C18:1,S)	38/103 (**36.9%**)	16/91 (**17.6%**) *
LCO-V(C18:1, Fuc/MeFuc)	24/140 (**17.1%**)	9/130 (**6.9%**) *

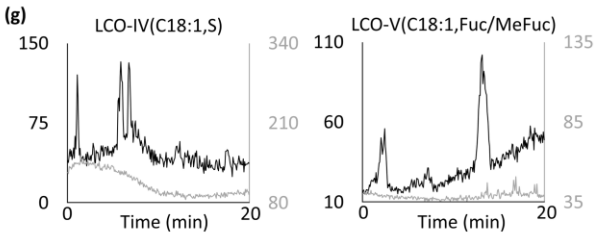

Figure 4. LCO induction of Ca^{2+} spiking in inner cell layers of tomato roots is partially *SlLYK10* dependent.

(a) Scheme of a tomato root section (not at scale) and focal planes used for imaging different root cell layers expressing G-GECO and DsRed (visible in green and red channels respectively). The red fluorescence in the center of the transversal focal plane corresponds to the auto-fluorescence of the vasculature. Scale bars represent 50µm. Separated green and red channels are shown in Supp Figure 4. (b) Representative green (black line, left y-axis) and red (grey line, right y-axis) fluorescence traces over time (x-axis) in nuclei visible in tangential focal planes of roots from G-GECO-DsRed tomato lines following treatment with 10^{-7} M CO4. Fluorescence measurements started 30 min after treatment and lasted 20 min. (c) Number of nuclei showing Ca^{2+} spiking to all fluorescent nuclei in root tangential focal planes following treatments with 10^{-7} M of the indicated chitinic signal molecules or ethanol (control) used as solvent for the stock solutions. Data are the sum from at least three independent plants. Only nuclei with two and more spikes along the 20 min were considered as responding cells. (d) Representative green (black line, left y axis) and red (grey line, right y axis) fluorescence traces over time (x axis) in transversal focal planes of roots from G-GECO-DsRed tomato lines following treatments with 10^{-7} M of the indicated chitinic signal molecules or ethanol (control). Measurement as in (b). (e) Number and proportion of nuclei showing Ca^{2+} spiking to all fluorescent nuclei in root transversal focal plans. Experimental design and counting as in (c).

(f) Number and proportion of nuclei showing Ca^{2+} spiking to all fluorescent nuclei in transversal focal planes on roots from segregating homozygote *Slyk10-1**G-GECO-DsRed (*Sllyk10-1*) or *SlLYK10**G-GECO-DsRed (Seg WT) plants. Experimental design and counting as in (c). Statistical differences between mutant and WT plants were calculated using a Chi-square test. * p-value < 0.05. (g) Representative green (black line, left y axis) and red (grey line, right y axis) fluorescence traces over time (x axis) in nuclei visible in transversal focal planes of roots from homozygote *Slyk10-1**G-GECO-DsRed plants. Treatment and measurement as in (d).

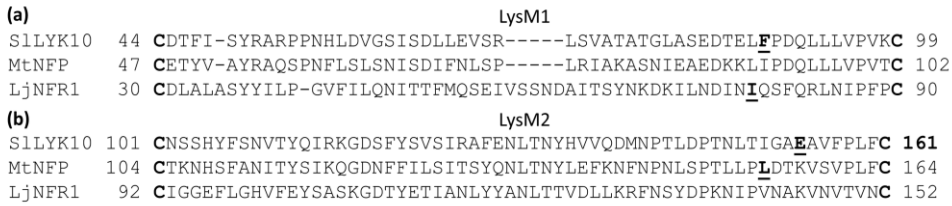

Figure 5. Position of residues with known functions on LysM-RLK alignments. SlLYK10, MtNFP and LjNFR1 LysM1 and 2 were alignment with Clustal Omega. Cys residues involved in di-sulphide bridges that delimit the LysMs are shown in bold. Residues shown to be critical for the protein functions (Bensmihen etal. 2011; Gysel et al. 2021 for MtNFP and Bozsoki et al. 2020 for LjNFR1) are shown in bold and underlined.